

Single-Photon Transport in a Topological Waveguide from a Dynamically Modulated Photonic System

Luoja Wang,¹ Luqi Yuan^{1,*} Xianfeng Chen^{1,2} and Shanhui Fan³

¹*State Key Laboratory of Advanced Optical Communication Systems and Networks, School of Physics and Astronomy, Shanghai Jiao Tong University, Shanghai 200240, China*

²*Collaborative Innovation Center of Light Manipulations and Applications, Shandong Normal University, Jinan 250358, China*

³*Department of Electrical Engineering, and Ginzton Laboratory, Stanford University, Stanford, California 94305, USA*



(Received 8 April 2020; revised 4 June 2020; accepted 9 June 2020; published 21 July 2020)

The topologically protected one-way edge modes for light show a way to manipulate the interaction between a single photon and a quantum emitter. We systematically study single-photon quantum optics in a *topological waveguide* supporting the frequency-dependent one-way edge mode at the boundary of a dynamically modulated photonic system, and compare the results of the single-photon interacting dynamics with the quantum emitter in a unidirectional waveguide. As a major difference, a photon in a topological waveguide propagates around the resonant site coupled to the quantum emitter due to the topological protection. Our results show that, despite different subtleties, photon-emitter interactions for one photon at the edge mode and for one photon propagating in a unidirectional waveguide hold similar features. In addition, we consider the interaction between the photon and a Λ -type three-level quantum emitter in the topological waveguide, where we show the nonlocal correlated photon-state generation as well as the single-photon reflection with the frequency conversion. Our work provides insight for understanding the interaction between the topologically protected unidirectional-propagating photon and the quantum emitter, which holds promise for potential applications in quantum-information processing.

DOI: 10.1103/PhysRevApplied.14.014063

I. INTRODUCTION

Manipulation of the interaction between a single photon and a quantum emitter is beneficial for quantum-information processing, which has attracted great interest in the field of quantum optics [1]. Strong coupling can be achieved in the waveguide quantum electrodynamics platform, where the photon state in a waveguide interacts strongly with a quantum emitter [2–15]. In particular, recent developments in photonic nanostructures make a chiral photon-emitter interacting process possible, which leads to the research field of chiral quantum optics pointing to the nonreciprocal control of light-matter interaction [16–21]. Among different technologies, the construction of a specially engineered photonic crystal waveguide shows an efficient way to couple the photon with the directionality dependent on the helicity of the transition of the quantum emitter [19].

Topological photonics has been extensively explored, where the topologically protected one-way edge states provide a powerful approach for generating unidirectional

photon transport that is robust against disorders [22]. It has been found that all-dielectric materials can be used to design topological photonic structures [23,24], supporting helical edge states with photon spin-dependent propagation directions [25]. Such helical edge states, when coupled with a nonreciprocal quantum emitter, can be used to achieve chiral single-photon quantum optics [25]. Moreover, topological one-way waveguide is capable in design at microwave frequencies in Weyl systems with the protection by the second Chern number [26]. On the other hand, one-way edge states can also be created using the effective gauge field generated by dynamically modulating photonic structures with proper phase distributions in either spatial space [27–29] or synthetic space [30–34]. In this dynamic photonic structure, the topologically protected one-way edge states can be prepared on demand.

In this paper, we study single-photon quantum optics in dynamically modulated photonic structures supporting one-way edge states and hence forming topological waveguides. Even though one-way edge states exist on the edge of a two-dimensional system [35], we show that light-matter interaction in these one-way edge states can be largely described using a one-dimensional chiral

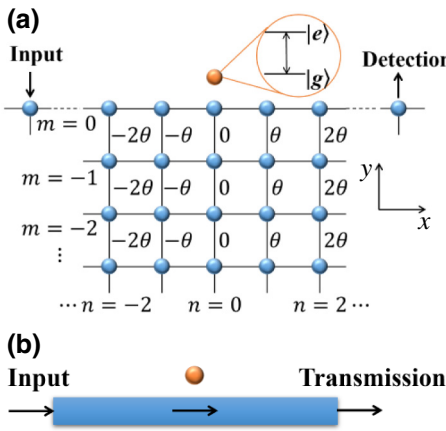
*yuanluqi@sjtu.edu.cn

waveguide model. In addition, we consider the photon-atom interaction of a Λ -type three-level atom in the topological waveguide where we explore the nonlocal correlated photon-state preparation and study the frequency conversion process. Our work provides a theoretical approach to study properties of single-photon transport in topological waveguides, and highlight some of the opportunities for the manipulation of the single-photon transport as created from the tunability in dynamically modulated photonic structures. Such opportunities are potentially useful for quantum communication and quantum computation [36–39].

II. FORMALISM

We start with introducing formalisms for photon-emitter interactions in the topological waveguide and the one-dimensional unidirectional waveguide, respectively. Here, by *topological waveguides*, we refer to the edge states of a two-dimensional system in Fig. 1(a). The Hamiltonian (1) then describes a two-dimensional system. In contrast, by one-dimensional *unidirectional waveguide*, we consider a true one-dimensional system in Fig. 1(b), which can be described by the one-dimensional Hamiltonian (6).

We first consider a topological waveguide, which can be achieved in photonic systems undergoing dynamic modulations. As shown in Fig. 1(a), the distribution of modulation phases being $\theta_n = n\theta$ along the x axis gives the effective magnetic field, where n is an integer labeling the site number along the x direction. Such a lattice can be achieved either in a two-dimensional photonic crystal [27] or a one-dimensional ring resonator array [31] with the refractive index of resonators being modulated. For the latter case, the square lattice shown in Fig. 1(a) is in the synthetic space, where the vertical axis gives the synthetic dimension along the frequency axis. Moreover, artificial boundary can be constructed along the frequency axis of light [33] and the transition frequency of the quantum emitter is assumed to be only near-resonant with the resonant



frequency at the artificial boundary. At the upper boundary, we place a two-level quantum emitter (or atom), with the excited state $|e\rangle$ and the ground state $|g\rangle$, coupling with the lattice at the site $(m, n) = (0, 0)$, where m is an integer labeling the lattice site along the y axis. Such a system can be described by the Hamiltonian [27,31]:

$$\begin{aligned} H = & \sum_{m,n} g \left(c_{m,n+1}^\dagger c_{m,n} + c_{m+1,n}^\dagger c_{m,n} e^{-in\theta} + \text{H.c.} \right) \\ & + \sum_{m,n} \omega_0 c_{m,n}^\dagger c_{m,n} + \omega_{eg} |e\rangle \langle e| \\ & + \kappa \left(c_{0,0}^\dagger + c_{0,0} \right) (\sigma_+ + \sigma_-), \end{aligned} \quad (1)$$

where $c_{m,n}^\dagger (c_{m,n})$ is the Bosonic creation (annihilation) operator for optical mode on the site (m, n) , $\sigma_{+(-)}$ is the atomic raising (lowering) ladder operator, ω_0 is the resonant frequency for the mode on the site (m, n) , and ω_{eg} is the atomic transition frequency. g corresponds to the coupling strengths between two nearest-neighbor sites and κ corresponds to the interaction strength between the quantum emitter and the optical mode at the site $(0, 0)$. Here, we set $\hbar = 1$ for simplicity. Under the rotating-wave approximation, the Hamiltonian, Eq. (1), becomes

$$\begin{aligned} H_{\text{RWA}} = & \sum_{m,n} g \left(c_{m,n+1}^\dagger c_{m,n} + c_{m+1,n}^\dagger c_{m,n} e^{-in\theta} + \text{H.c.} \right) \\ & + \Delta |e\rangle \langle e| + \kappa \left(c_{0,0}^\dagger \sigma_- + c_{0,0} \sigma_+ \right), \end{aligned} \quad (2)$$

where we define the detuning $\Delta = \omega_{eg} - \omega_0$. The single-excitation state of the topological-waveguide system is

$$|\Psi\rangle = \sum_{m,n} v_{m,n}(t) c_{m,n}^\dagger |0,g\rangle + w(t) |0,e\rangle, \quad (3)$$

where $v_{m,n}$ is the probability amplitude at the site (m, n) and w is the probability amplitude for the quantum emitter

FIG. 1. (a) Schematic of a two-level quantum emitter interacting with a topological waveguide, which is achieved by a stripe of a dynamically modulated photonic resonator lattice subjected to an effective magnetic field. (b) Schematic of a quantum emitter coupled to a non-reciprocal unidirectional waveguide. (c) Band structure of the photonic lattice under the dynamical modulation. The red (green) curve indicates the right-(left-) propagating edge state at the top boundary of the lattice.

at the excited state. The Schrödinger equation $i\partial|\Psi\rangle/dt = H_{\text{RWA}}|\Psi\rangle$ yields the following equations of motion:

$$\begin{aligned}\dot{v}_{m,n}(t) &= -ig[v_{m,n-1}(t) + v_{m,n+1}(t) + v_{m-1,n}(t)e^{-in\theta} \\ &\quad + v_{m+1,n}(t)e^{in\theta}] - i\kappa w(t)\delta_{m0}\delta_{n0},\end{aligned}\quad (4)$$

$$\dot{w}(t) = -i\Delta w(t) - i\kappa v_{0,0}(t). \quad (5)$$

For comparison, we also model the photon-emitter interaction in the unidirectional waveguide as shown in Fig. 1(b). Under the linear-dispersion approximation and the rotating-wave approximation, the real-space Hamiltonian that describes this system takes the form [2,21,40]

$$\begin{aligned}H &= \int dx \left\{ -iv_g c_R^\dagger(x) \frac{\partial}{\partial x} c_R(x) \right. \\ &\quad \left. + \kappa\delta(x) [c_R^\dagger(x)\sigma_- + \sigma_+ c_R(x)] \right\} + \Delta |e\rangle\langle e|,\end{aligned}\quad (6)$$

where $c_R^\dagger(x)$ is the creation operator that creates a right-propagating photon at x , and $c_R(x)$ is the corresponding annihilation operator. The single-excitation state of the unidirectional waveguide system is

$$|\Psi\rangle = \int dx \phi_R(t,x) c_R^\dagger(x) |0,g\rangle + w(t) |0,e\rangle. \quad (7)$$

Hence, with the Schrödinger equation, $\phi_R(t,x)$ and $w(t)$ follow the equations of motion:

$$\left(\frac{\partial}{\partial t} + v_g \frac{\partial}{\partial x} \right) \phi_R(t,x) = -i\kappa\delta(x) w(t), \quad (8)$$

$$\dot{w}(t) = -i\Delta w(t) - i\kappa \int dx \delta(x) \phi_R(t,x). \quad (9)$$

We then use the formalisms established above to explore the single photon interacting with the two-level quantum emitter in the topological waveguide and the unidirectional waveguide, respectively, by numerically solving Eqs. (4), (5) and (8), (9). For the topological waveguide platform, we choose a lattice size 10×51 , where $m = 0, -1, \dots, -9$, $n = -25, -24, \dots, 25$, and $\theta = 0.5\pi$. The choice of the phase distribution supports an effective magnetic field and hence breaks the time-reversal symmetry of the system. The topological properties can be shown from the band structure as shown in Fig. 1(c), which is calculated by considering a strip with $m \in [-50, 0]$ and n being infinite. The band structure is plotted versus the wavevector k_x , showing topologically protected edge states in gaps between bulk bands [27,31]. In particular, as labeled in color in Fig. 1(c), there are a pair of edge states on the

upper boundary of the lattice, with different (right- and left-propagating) directionalities. The wavepacket of the single photon is injected at the site $(0, -8)$, with the carrier frequency shift $\varepsilon = \omega_c - \omega_0 = -2g$ and the pulse bandwidth $\delta_W = 0.089g$, to excite the right-propagating edge state. The two-level quantum emitter is chosen to be resonant with the carrier frequency of the photon ($\omega_{eg} - \omega_c = 0$) and has the interaction strength $\kappa = 0.2g$ in our simulations. Therefore, the initial state can be written as $|\Psi(0)\rangle = |0,g\rangle$. The transmitted signal is collected at the site $(0, 6)$.

III. PHOTON TRANSPORT IN WAVEGUIDES INTERACTING WITH A TWO-LEVEL ATOM

Figure 2(a) shows the spectra of the transmitted wave in the topological waveguide without the atom ($|E_T^0(\omega_{eg} - \omega)|$) and transmitted wave ($|E_T(\omega_{eg} - \omega)|$) for the photon propagating through the waveguide interacting with the atom. One can see that the transmitted spectrum follows the Gaussian shape, which gives a 100% transmission due to the one-way feature of the edge mode. For the frequency component near ω_{eg} , the pulse of the photon experiences highly dispersive propagation due to the coupling with the quantum emitter. Since the quantum emitter is populated at the ground state for the initial and final stage, the transmission process in this system can be treated as a linear system, with the frequency response defined as $H(\omega) \equiv E_T(\omega)/E_I(\omega)$, where $E_I(\omega)$ is the incident spectrum. One hence has the standard group delay as [41]

$$t_g(\omega) = \frac{d\Phi(\omega)}{d\omega}, \quad (10)$$

where $\Phi(\omega) = -\text{Arg}H(\omega)$, indicating the time delay of the peak of pulse traveling through the system. We plot

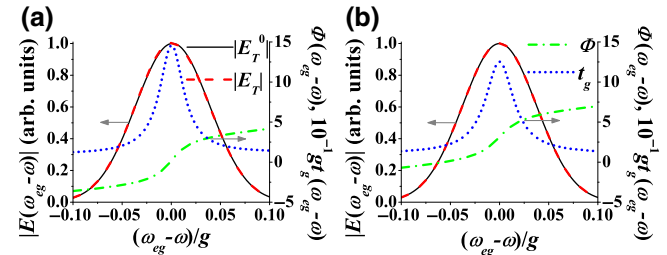


FIG. 2. Single-photon transport dynamics in (a) the topological waveguide and (b) the unidirectional waveguide, with transmitted field spectra of waveguides interacting with the atom ($|E_T|$, red dash lines) compared to waveguides without the atom ($|E_T^0|$, black solid lines) against the left vertical axis, the spectral phase (Φ , green dash-dotted lines) and the group delay (t_g , blue dotted lines) for the transmitted field in the waveguide interacting with the atom against the right vertical axis. The atomic transition frequency is $\omega_{eg} = \omega_c$ and the interaction strength is $\kappa = 0.2g$.

$t_g(\omega_{eg} - \omega)$ and $\Phi(\omega_{eg} - \omega)$ in Fig. 2(a). One can see the maximum of t_g is at the transition frequency of the quantum emitter. In simulations, one finds that the photon propagating through the upper boundary of the lattice unidirectionally without scattering back by the defect, which is the site $(0, 0)$ coupled with the quantum emitter in this case. Moreover, the photon is absorbed by the quantum emitter even though it propagates following the edge state of the system, and then is re-emitted by the quantum emitter, which exhibits features of the group delay in plots.

To understand the transport features in the topological waveguide, we next simulate the photon-emitter interaction in a unidirectional waveguide and compare results in both platforms. Equations (8) and (9) are used to perform simulations with the same parameters, but $v_g = 1.15a \times g$ with a being the lattice spacing of the topological waveguide such that the pulse propagating in the unidirectional waveguide without the quantum emitter exhibits the same group velocity as that in the topological waveguide. The initial state is $|\Psi(0)\rangle = |0, g\rangle$. Simulation results are plotted in Fig. 2(b). One notices that the properties of the spectra and the group delays are similar to those for the topological waveguide, except for an additional spectral phase. Nevertheless, there is a natural question arising in the comparison of photon transports in topological and unidirectional waveguides: in the topologically protected edge mode, the photon is supposed to propagate around the defect, i.e., the site $(0, 0)$ where the emitter is coupled, which is different from the chiral mode in the unidirectional waveguide, where the photon propagates through the position at $x = 0$ and interacts with the quantum emitter directly. Therefore, does the photon still interact efficiently with the quantum emitter, which is coupled with the site $(0, 0)$ in the topological waveguide? To address this question, in the following we study the parameter regime in detail.

In Fig. 3, we show changes of the delay τ between the emitted field and the input field (which is defined in the inset) as well as the total excitation, $\int \rho_{ee} dt$, for two types of waveguides, and also the normalized comparisons $\Delta\tau/\tau = (\tau_{\text{topological}} - \tau_{\text{unidirectional}})/\tau_{\text{topological}}$ and similarly defined $\Delta \int \rho_{ee} dt / \int \rho_{ee} dt$ between two waveguides versus κ . One can see that the delay τ is large for smaller κ , and it decays towards zero once κ is increased. The relative difference $\Delta\tau/\tau$ shows that it is almost zero for smaller κ but it goes up to approximately 15% for $\kappa \approx g$. The total excitation of the quantum emitter shows a relatively large excitation when $\kappa \sim 0.1g$. For $\kappa \sim g$, it goes to zero. The relative difference in two waveguides shows approximately -5% at $\kappa = 0.1g$, decreases to approximately 0 at $\kappa \approx 0.22g$, and then increases to approximately 8% at $\kappa \sim g$.

The dependencies of the group delay $t_g(\omega_{eg} - \omega)$ versus κ are shown in Fig. 4. One can see that t_g in both waveguides exhibit a positive group delay for the majority

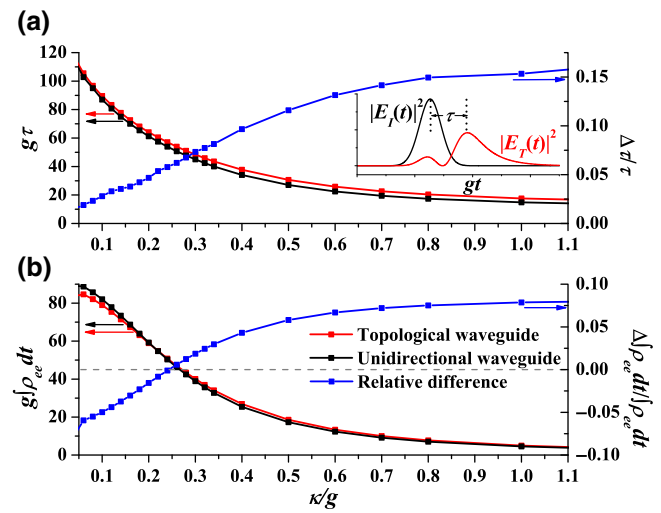


FIG. 3. (a) Delay τ (defined as the schematic in the inset), and (b) the total excitation $\int \rho_{ee} dt$ for the topological waveguide (red) and the unidirectional waveguide (black) versus the interaction strength κ . The relative differences (blue) between two types of waveguides defined in the text are also given against the right vertical axis.

of the parameter regime in the ω - κ space, but a large peak near the resonant frequency $\omega \approx \omega_{eg}$ for small κ . In Fig. 4(c), we also plot the normalized comparison $\Delta t_g/t_g = (t_{g,\text{topological}} - t_{g,\text{unidirectional}})/t_{g,\text{topological}}$. It shows that the relative difference $\Delta t_g/t_g$ gives a positive value up to approximately 17% for large κ , while gives the negative value for smaller κ at the nonresonant frequency. With the proper choice of parameter, one can find the difference $\Delta t_g \rightarrow 0$ between two waveguides. The group delay exhibits a symmetric pattern over the detuning $\omega_{eg} - \omega$ for the unidirectional waveguide [see Fig. 4(b)]. However, t_g does not give a symmetric pattern for the topological waveguide, because the dispersion of the excited edge mode is not linear. Besides these subtleties with $< 20\%$ difference discussed above, the overall features are very similar in both waveguides.

The last question remaining is how to understand the interaction between the light and the emitter while the defect is introduced by the emitter and the topological edge mode is supposed to propagate around it. We show the typical distribution of the field in a topological waveguide for $\kappa = 0.2g$ in Fig. 5(a), which is a snapshot in the simulation at $t = 164.95g^{-1}$. The field intensity $|E_B|^2$ at the site $(0, -1)$, which is beneath the site $(0, 0)$, gives a maximum value around this specific time. We see that the edge mode of the field propagates around the lattice site $(0, 0)$. Figure 5(b) plots the normalized total intensity of $|E_B|^2$ versus κ . For smaller κ , the intensity is relatively small, and it gradually increases and becomes saturated at $\kappa \sim 0.6$. This behavior is consistent with the change of the excited population in Fig. 3(b), as for smaller κ , more population

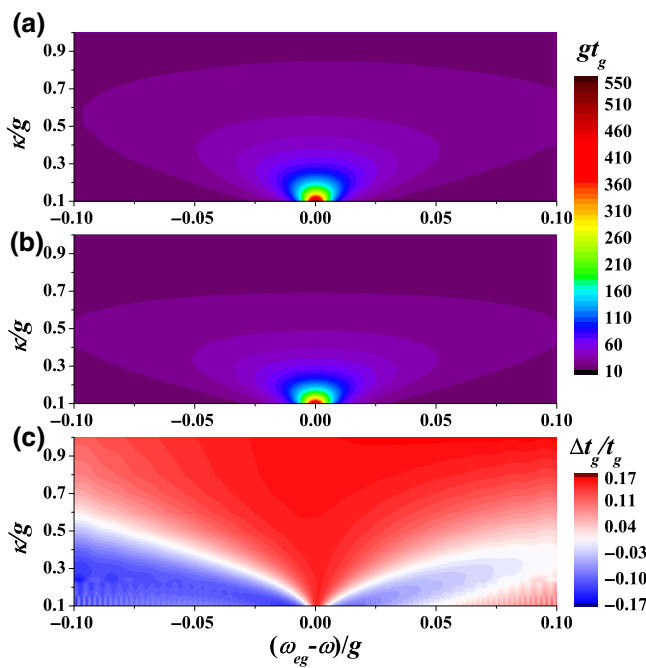


FIG. 4. Group delay t_g in (a) the topological waveguide, (b) the unidirectional waveguide, and (c) the relative difference of the group delay $\Delta t_g/t_g$ between two types of waveguides versus $\omega_{eg} - \omega$ and κ .

is excited while less field goes through the site $(0, -1)$. These results give reasonable explanations: for larger κ , the defect from the emitter behaves strongly, so the edge mode is propagating around the defect and the excitation of the emitter is small; on the other hand, for smaller κ , such a defect disturbs the system weakly, and hence light can propagate through the site $(0, 0)$ and interact directly with the emitter.

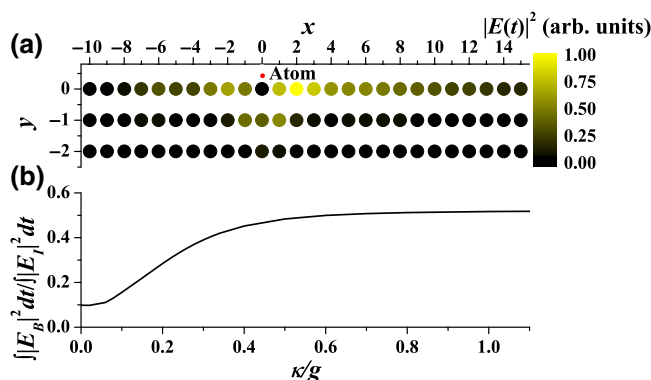


FIG. 5. (a) Snapshot of field-intensity distribution in a topological waveguide for $\kappa = 0.2g$ and $t = 164.95g^{-1}$. The lattice site interacting with the resonant quantum emitter is indicated. (b) Normalized total intensity of the field at the site $(0, -1)$ beneath the interacting site $(0, 0)$ versus κ .

IV. CORRELATED PHOTON STATE GENERATION

Due to the similarity of photon-matter interactions in both the topological waveguide and the unidirectional waveguide, the topological waveguide gives a good candidate for manipulating the single-photon state. In this section, as an example, we show that one can generate a correlated single-photon state in the topological waveguide coupled with a Λ -type quantum emitter, where two modes of the photon correspond to two edge modes at the same edge, but with opposite directionalities and with different frequencies, shown in Fig. 1(c). Here, the single-photon state reads

$$|\Psi_s\rangle = \frac{1}{\sqrt{1+|\eta|^2}} (|1_L 0_R\rangle + \eta |0_L 1_R\rangle), \quad (11)$$

where the state $|1_L 0_R\rangle$ ($|0_L 1_R\rangle$) describes one photon propagating towards left (right) while no photon propagating towards right (left). $|\eta|^2$ corresponds to the ratio between two states. Equation (11) describes a nonlocal correlated photon state. This state is analogous to a state that is generated by sending a single photon through a beam splitter [36], and hence $|\eta|^2$ can be associated to the reflectivity of the beam splitter. However, here in the state of Eq. (11) the two basis states are at different frequencies. Successful preparation of such a correlated single-photon state in Eq. (11) with different $|\eta|^2$ is useful for demonstrating quantum logic gates [42–46] and for developments of quantum technologies in quantum communication [47] and quantum computation [48].

To generate the correlated single-photon state in Eq. (11), we propose a Λ -type quantum emitter coupled with the site $(0, 0)$ in the topological waveguide we discuss above [see Fig. 6(a)]. The system can be described by the Hamiltonian:

$$\begin{aligned} H = & \sum_{m,n} g \left(c_{m,n+1}^\dagger c_{m,n} + c_{m+1,n}^\dagger c_{m,n} e^{-in\theta} + \text{H.c.} \right) \\ & - \Delta_1 |g_1\rangle \langle g_1| - \Delta_2 |g_2\rangle \langle g_2| \\ & + \kappa_1 \left(c_{0,0}^\dagger \sigma_{1-} + c_{0,0} \sigma_{1+} \right) + \kappa_2 \left(c_{0,0}^\dagger \sigma_{2-} + c_{0,0} \sigma_{2+} \right), \end{aligned} \quad (12)$$

where $\kappa_{1(2)}$ denotes the interaction strength between the transition $|e\rangle \leftrightarrow |g_{1(2)}\rangle$ and the optical mode at the site $(0, 0)$. ω_0 is chosen to be the corresponding zero energy point in the band structure shown in Fig. 1(c). $\Delta_{1(2)} = \omega_{eg_{1(2)}} - \omega_0$. We consider the state of the system as

$$\begin{aligned} |\Psi\rangle = & \sum_{m,n} v_{m,n}^1(t) c_{m,n}^\dagger |0, g_1\rangle \\ & + \sum_{m,n} v_{m,n}^2(t) c_{m,n}^\dagger |0, g_2\rangle + w(t) |0, e\rangle, \end{aligned} \quad (13)$$

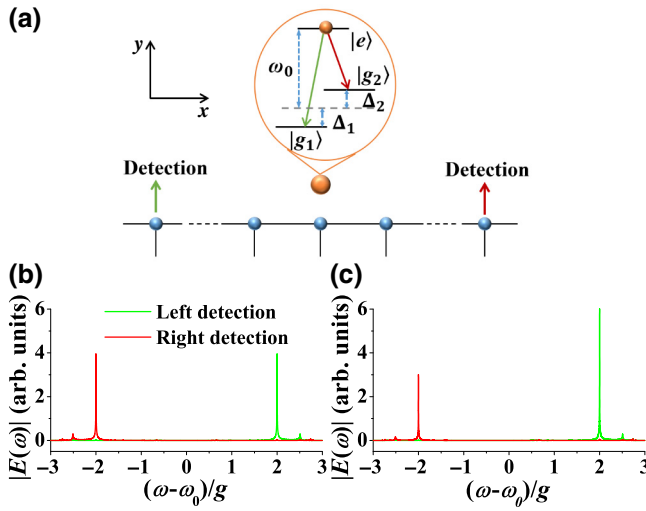


FIG. 6. (a) Schematic of an initially excited Δ -type quantum emitter interacting with a topological waveguide under the dynamical modulation. The spectra of the detected fields at the left (green) and right (red) detection points for (b) $\kappa_1 = \kappa_2 = 0.05g$ and (c) $\kappa_1 = 2\kappa_2 = 0.05g$.

and perform simulations with initially preparing the quantum emitter populated at the excited state $|e\rangle$, which can be achieved by driving the quantum emitter with a classical pump pulse. There is no input photon and we place two detectors at sites $(0, -6)$ and $(0, 6)$, respectively. Parameters for the topological waveguide here are chosen to be the same as those in the simulation for Fig. 2. For transitions in the quantum emitter, we set $\Delta_1 = 2g$ and $\Delta_2 = -2g$, which corresponds to the edge states in the top and bottom gaps in Fig. 1(c), respectively.

We plot the simulation results with $\kappa_1 = \kappa_2 = 0.05g$ and $\kappa_1 = 2\kappa_2 = 0.05g$ in Figs. 6(b) and 6(c), respectively. For the case with $\kappa_1 = \kappa_2$, one can see that the signal at the left detector shows a major peak near the frequency shift $2g$ while the signal at the right detector shows a major peak near the frequency shift $-2g$. Two peaks at the same strength indicate that the possibilities of generating the photon at the frequency shift $\pm 2g$ propagating towards left and right are the same. Since there is only one quantum emitter coupled with the topological waveguide, only one photon can be generated at a certain time window. Hence, we demonstrate the generation of the correlated photon state in Eq. (11) with $|\eta|^2 = 1$. As for the case with $\kappa_1 = 2\kappa_2$, one notices that the peak of the signal from the left detector is larger than the peak from the right detector. Therefore, it corresponds to the single-photon state Eq. (11) with $|\eta|^2 = 0.25$.

The phase difference between the left-propagating photon state and the right-propagating photon state is fixed. In principle, it can be adjusted by designing dipoles between transitions $|e\rangle \leftrightarrow |g_{1(2)}\rangle$ in the quantum emitter carrying

extra phase factors. Moreover, the edge states are topologically protected [27,31] in our proposal for the generation of such a nonlocal correlated photon state with the extra tunability of $|\eta|^2$. Such a state consisting of a linear superposition of a single photon propagating at two different directions can not be achieved in the unidirectional waveguide considered above. The frequency difference between two states can reach from 10 MHz to 10 GHz in the dynamically modulated photonic systems [49–53]. Moreover, it does not require radiative transitions in the quantum emitter with opposite polarizations under the magnetic field [25].

V. SINGLE-PHOTON REFLECTION WITH THE FREQUENCY CONVERSION

In this section, we study the interaction between an injected photon inside the topological waveguide and the same Δ -type quantum emitter described in Fig. 6(a) in the previous section. We choose the injected photon to be resonant with one of the transition in the emitter and explore the critical coupling conditions for the reflection of the single-photon state with its frequency getting converted. In our numerical setup, we assume that the quantum emitter is initially prepared in one of ground states, i.e., $|g_2\rangle$. A Gaussian pulse with the central frequency at $\omega_0 - 2g$ (resonant with the transition $|e\rangle \leftrightarrow |g_2\rangle$) and the width $\delta_W = 0.08g$ is injected from the left side of the topological waveguide, which excites the corresponding right-propagating edge mode. The photon can therefore excite the emitter and the resulting emission gives either a right-propagating photon at the input frequency or a left-propagating photon in the vicinity of the frequency $\omega_0 + 2g$.

In Fig. 7, we summarize the simulation results with a fixed $\kappa_2 = 0.1g$, $0.2g$, respectively, and κ_1 being tuned. Figures 7(a) and 7(b) plot the normalized spectra of the left-propagating emission and right-propagating emission for $\kappa_2 = 0.1g$ and $\kappa_2 = 0.2g$ with $\Delta\omega_{R(L)} \equiv \omega - \omega_0 + (-)2g$. For the left-propagation reflection, the frequency of the photon state is shifted. One can see that there is a dip for the spectrum of the right-propagating emission and a hip for the spectrum of the left-propagating emission near the resonance. The width of the dip (hip) is dependent on both κ_1 and κ_2 . Nevertheless, the dip for the right-propagating transmitted spectrum drops to zero only for the case $\kappa_1 = \kappa_2$ for both $\kappa_2 = 0.1g$ and $\kappa_2 = 0.2g$ on the resonance, where the reflection is up to 1 but its frequency is changed. To better see the critical coupling condition for the frequency conversion in the system, we plot the field amplitude corresponding to the right and left emission at the resonance ($\Delta\omega_{R/L} = 0$) versus κ_1 in Figs. 7(c) and 7(d) for $\kappa_2 = 0.1g$ and $\kappa_2 = 0.2g$, respectively. The critical coupling indeed happens at $\kappa_1 = \kappa_2$. It indicates that the input photon at the frequency $\omega_0 - 2g$ propagating

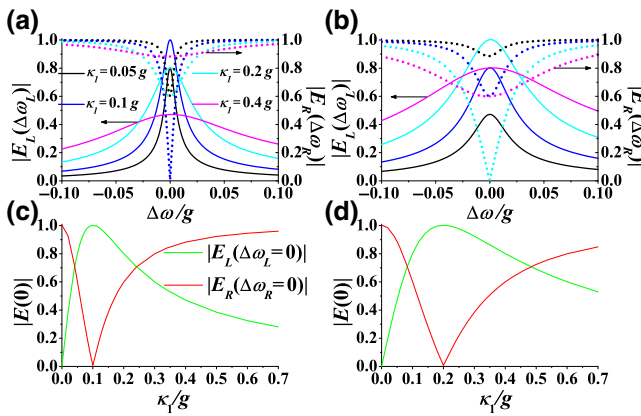


FIG. 7. Normalized spectra of the output left-propagating emission (solid lines against the left vertical axis) versus $\Delta\omega_L$ and the output right-propagating emission (dotted lines against the right vertical axis) versus $\Delta\omega_R$ for (a) $\kappa_2 = 0.1g$ and (b) $\kappa_2 = 0.2g$, with varying $\kappa_1 = 0.05g$ (black), $0.1g$ (blue), $0.2g$ (cyan), and $0.4g$ (magenta). $\Delta\omega_{R(L)} \equiv \omega - \omega_0 + (-)2g$. The resonant amplitude of the output left-propagating emission (green) and the output right-propagating emission (red) versus κ_1 for (c) $\kappa_2 = 0.1g$ and (d) $\kappa_2 = 0.2g$. The spectra are normalized by the transmitted spectra as a function of $\Delta\omega_R$ in a topological waveguide without the atom.

towards the right can be fully transferred to an emitted photon at the frequency $\omega_0 + 2g$ propagating towards the left. Here, we demonstrate the frequency upshift while a right-propagating single photon is fully reflected. Similarly, a left-propagating photon resonant with the $|e\rangle \leftrightarrow |g_1\rangle$ transition can also get fully reflected while its frequency is downshifted.

Moreover, we consider that the physical system is unchanged but all signs of phases in external modulations are changed. In this case, the direction of the effective magnetic flux is flipped, and then the edge mode near the resonant frequency $\omega_0 + 2g$ is right propagating while the edge mode near $\omega_0 - 2g$ is left propagating. Hence, all spectra studied above for the single photon interacting with the Λ -type quantum emitter inside the topological waveguide will be flipped with the mirror symmetry.

VI. SUMMARY

In summary, we provide a detailed schematic theoretical study of the single-photon interacting dynamics with the quantum emitter in different types of waveguides. In particular, we consider a topological waveguide, which is associated with the one-way edge mode at the boundary of a dynamically modulated photonic system. The lattice size of such a two-dimensional photonic system is quite flexible for potential experimental implementations since signatures of edge states preserve if one decreases the number of layers of the lattice [53]. By placing a two-level quantum emitter inside the waveguide, the transport property of the

single photon exhibits a similar feature to that in a unidirectional waveguide, regardless of the fact that the topological protection makes the wavepacket of the photon transmit around the defect, i.e., the resonant site coupled with the quantum emitter. Different to the topological chiral waveguide, where photon with different chirality propagates at opposite directions [25], the dynamically modulated photonic systems potentially provide reconfigurable functionality [54] and exhibit frequency-dependence one-way edge modes. It therefore provides a unique platform for us to propose the generation of the nonlocal correlated photon, where the system serves both functionalities of the photon generation and the beam splitter with the tunable reflectivity and hence exhibits potential applications in quantum communication and quantum computation. Moreover, one can achieve the full reflection of a single photon with its frequency converted. Our work serves the purpose for understanding the interaction between the topologically protected unidirectional-propagating photon and the quantum emitter, and holds promise for future applications towards quantum-information processing in the photonic platform with the rapid-developing dynamic modulation technologies in the real space [49–51,55,56] and in the synthetic space [52,53].

ACKNOWLEDGMENTS

This paper is supported by National Natural Science Foundation of China (Grant No. 11974245), National Key R&D Program of China (Grants No. 2018YFA0306301 and No. 2017YFA0303701), Natural Science Foundation of Shanghai (Grant No. 19ZR1475700). This work is also partially supported by the U.S. National Science Foundation Grant No. CBET-1641069.

- [1] D. E. Chang, J. S. Douglas, A. González-Tudela, C.-L. Hung, and H. J. Kimble, Colloquium: Quantum matter built from nanoscopic lattices of atoms and photons, *Rev. Mod. Phys.* **90**, 031002 (2018).
- [2] J.-T. Shen and S. Fan, Coherent Single Photon Transport in a One-Dimensional Waveguide Coupled with Superconducting Quantum Bits, *Phys. Rev. Lett.* **95**, 213001 (2005).
- [3] S. Fan, Ş. E. Kocabas, and J.-T. Shen, Input-output formalism for few-photon transport in one-dimensional nanophotonic waveguides coupled to a qubit, *Phys. Rev. A* **82**, 063821 (2005).
- [4] S. Xu and S. Fan, Generalized cluster decomposition principle illustrated in waveguide quantum electrodynamics, *Phys. Rev. A* **95**, 063809 (2017).
- [5] A. V. Akimov, A. Mukherjee, C. L. Yu, D. E. Chang, A. S. Zibrov, P. R. Hemmer, H. Park, and M. D. Lukin, Generation of single optical plasmons in metallic nanowires coupled to quantum dots, *Nature* **450**, 402 (2007).

- [6] H. Zheng, D. J. Gauthier, and H. U. Baranger, Waveguide-QED-Based Photonic Quantum Computation, *Phys. Rev. Lett.* **111**, 090502 (2013).
- [7] D. Roy and N. Bondyopadhyaya, Statistics of scattered photons from a driven three-level emitter in a one-dimensional open space, *Phys. Rev. A* **89**, 043806 (2014).
- [8] A. Goban, C.-L. Hung, S.-P. Yu, J. D. Hood, J. A. Muniz, J. H. Lee, M. J. Martin, A. C. McClung, K. S. Choi, D. E. Chang, O. Painter, and H. J. Kimble, Atom-light interactions in photonic crystals, *Nat. Commun.* **5**, 3808 (2014).
- [9] Z. H. Wang, L. Zhou, Y. Li, and C. P. Sun, Controllable single-photon frequency converter via a one-dimensional waveguide, *Phys. Rev. A* **89**, 053813 (2014).
- [10] Q. Li, L. Zhou, and C. P. Sun, Waveguide quantum electrodynamics: Controllable channel from quantum interference, *Phys. Rev. A* **89**, 063810 (2014).
- [11] T. Y. Li, J. F. Huang, and C. K. Law, Scattering of two distinguishable photons by a Xi-type three-level atom in a one-dimensional waveguide, *Phys. Rev. A* **91**, 043834 (2015).
- [12] Y. Shen and J.-T. Shen, Photonic-Fock-state scattering in a waveguide-QED system and their correlation functions, *Phys. Rev. A* **92**, 033803 (2015).
- [13] J. D. Hood, A. Goban, A. Asenjo-Garcia, M. Lu, S.-P. Yu, D. E. Chang, and H. J. Kimble, Atom-atom interactions around the band edge of a photonic crystal waveguide, *Proc. Natl. Acad. Sci. USA* **113**, 10507 (2016).
- [14] D. Roy, Critical features of nonlinear optical isolators for improved nonreciprocity, *Phys. Rev. A* **96**, 033838 (2017).
- [15] Z. Chen, Y. Zhou, and J.-T. Shen, Dissipation-induced photonic-correlation transition in waveguide-QED systems, *Phys. Rev. A* **96**, 053805 (2017).
- [16] P. Lodahl, S. Mahmoodian, S. Stobbe, A. Rauschenbeutel, P. Schneeweiss, J. Volz, H. Pichler, and P. Zoller, Chiral quantum optic, *Nature* **541**, 473 (2017).
- [17] C. Junge, D. O'Shea, J. Volz, and A. Rauschenbeutel, Strong Coupling between Single Atoms and Nontransversal Photons, *Phys. Rev. Lett.* **110**, 213604 (2013).
- [18] I. Shomroni, S. Rosenblum, Y. Lovsky, O. Bechler, G. Guendelman, and B. Dayan, All-optical routing of single photons by a one-atom switch controlled by a single photon, *Science* **345**, 903 (2014).
- [19] I. Söllner, S. Mahmoodian, S. L. Hansen, L. Midolo, A. Javadi, G. Kiršanskė, T. Pagnolato, H. El-Ella, E. H. Lee, J. D. Song, S. Stobbe, and P. Lodahl, Deterministic photon-emitter coupling in chiral photonic circuits, *Nat. Nanotechnol.* **10**, 775 (2015).
- [20] C. Sayrin, C. Junge, R. Mitsch, B. Albrecht, D. O'Shea, P. Schneeweiss, J. Volz, and A. Rauschenbeutel, Nanophotonic Optical Isolator Controlled by the Internal State of Cold Atoms, *Phys. Rev. X* **5**, 041036 (2015).
- [21] L. Yuan, S. Xu, and S. Fan, Achieving nonreciprocal unidirectional single-photon quantum transport using the photonic Aharonov–Bohm effect, *Opt. Lett.* **40**, 5140 (2015).
- [22] T. Ozawa, H. M. Price, A. Amo, N. Goldman, M. Hafezi, L. Lu, M. C. Rechtsman, D. Schuster, J. Simon, O. Zilberberg, and I. Carusotto, Topological photonics, *Rev. Mod. Phys.* **91**, 015006 (2019).
- [23] L.-H. Wu and X. Hu, Scheme for Achieving a Topological Photonic Crystal by Using Dielectric Material, *Phys. Rev. Lett.* **114**, 223901 (2015).
- [24] S. Barik, H. Miyake, W. DeGottardi, E. Waks, and M. Hafezi, Two-dimensionally confined topological edge states in photonic crystals, *New J. Phys.* **18**, 113013 (2016).
- [25] S. Barik, A. Karasahin, C. Flower, T. Cai, H. Miyake, W. DeGottardi, M. Hafezi, and E. Waks, A topological quantum optics interface, *Science* **359**, 666 (2018).
- [26] L. Lu, H. Gao, and Z. Wang, Topological one-way fiber of second Chern number, *Nat. Commun.* **9**, 5384 (2018).
- [27] K. Fang, Z. Yu, and S. Fan, Realizing effective magnetic field for photons by controlling the phase of dynamic modulation, *Nat. Photon.* **6**, 782 (2012).
- [28] K. Fang and S. Fan, Controlling the Flow of Light Using the Inhomogeneous Effective Gauge Field That Emerges from Dynamic Modulation, *Phys. Rev. Lett.* **111**, 203901 (2013).
- [29] Q. Lin and S. Fan, Light Guiding by Effective Gauge Field for Photons, *Phys. Rev. X* **4**, 031031 (2014).
- [30] D. Jukić and H. Bujian, Four-dimensional photonic lattices and discrete tesseract solitons, *Phys. Rev. A* **87**, 013814 (2013).
- [31] L. Yuan, Y. Shi, and S. Fan, Photonic gauge potential in a system with a synthetic frequency dimension, *Opt. Lett.* **41**, 741 (2016).
- [32] T. Ozawa, H. M. Price, N. Goldman, O. Zilberberg, and I. Carusotto, Synthetic dimensions in integrated photonics: From optical isolation to four-dimensional quantum Hall physics, *Phys. Rev. A* **93**, 043827 (2016).
- [33] L. Yuan, Q. Lin, A. Zhang, M. Xiao, X. Chen, and S. Fan, Photonic Gauge Potential in one Cavity with Synthetic Frequency and Orbital Angular Momentum Dimensions, *Phys. Rev. Lett.* **122**, 083903 (2019).
- [34] E. Lustig, S. Weimann, Y. Plotnik, Y. Lumer, M. A. Bandres, A. Szameit, and M. Segev, Photonic topological insulator in synthetic dimensions, *Nature* **567**, 356 (2019).
- [35] G. L. Giorgi, S. Lorenzo, and S. Longhi, Topological protection and control of quantum Markovianity, *Photonics* **7**, 18 (2020).
- [36] P. Kwiat, H. Weinfurter, T. Herzog, A. Zeilinger, and M. A. Kasevich, Interaction-Free Measurement, *Phys. Rev. Lett.* **74**, 4763 (1995).
- [37] P. G. Kwiat, A. G. White, J. R. Mitchell, O. Nairz, G. Weihs, H. Weinfurter, and A. Zeilinger, High-Efficiency Quantum Interrogation Measurements via the Quantum Zeno Effect, *Phys. Rev. Lett.* **83**, 4725 (1999).
- [38] O. Hosten, M. T. Rakher, J. T. Barreiro, N. A. Peters, and P. G. Kwiat, Counterfactual quantum computation through quantum interrogation, *Nature* **439**, 949 (2006).
- [39] T.-G. Noh, Counterfactual Quantum Cryptography, *Phys. Rev. Lett.* **103**, 230501 (2009).
- [40] J.-T. Shen and S. Fan, Theory of single-photon transport in a single-mode waveguide. I. Coupling to a cavity containing a two-level atom, *Phys. Rev. A* **79**, 023837 (2009).
- [41] S. J. Orfanidis, *Electromagnetic Waves and Antennas* (Rutgers University, Piscataway, NJ, USA, 2014).
- [42] A. Politi, M. J. Cryan, J. G. Rarity, S. Yu, and J. L. O'Brien, Silica-on-Silicon waveguide quantum circuits, *Science* **320**, 646 (2008).

- [43] A. Crespi, R. Ramponi, R. Osellame, L. Sansoni, I. Bonfiggiani, F. Sciarrino, G. Vallone, and P. Mataloni, Integrated photonic quantum gates for polarization qubits, *Nat. Commun.* **2**, 566 (2011).
- [44] D. Bonneau, E. Engin, K. Ohira, N. Suzuki, H. Yoshida, N. Iizuka, M. Ezaki, C. M. Natarajan, M. G. Tanner, R. H. Hadfield, S. N. Dorenbos, V. Zwiller, J. L. O'Brien, and M. G. Thompson, Quantum interference and manipulation of entanglement in silicon wire waveguide quantum circuits, *New J. Phys.* **14**, 045003 (2012).
- [45] R. Heilmann, M. Gräfe, S. Nolte, and A. Szameit, Arbitrary photonic wave plate operations on chip: Realizing Hadamard, Pauli-X, and rotation gates for polarisation qubits, *Sci. Rep.* **4**, 4118 (2014).
- [46] T. Meany, M. Gräfe, R. Heilmann, A. Perez-Leija, S. Gross, M. J. Steel, M. J. Withford, and A. Szameit, Laser written circuits for quantum photonics, *Laser Photon. Rev.* **9**, 363 (2015).
- [47] N. Gisin, G. Ribordy, W. Tittel, and H. Zbinden, Quantum cryptography, *Rev. Mod. Phys.* **74**, 145 (2002).
- [48] P. Kok, W. J. Munro, K. Nemoto, T. C. Ralph, J. P. Dowling, and G. J. Milburn, Linear optical quantum computing with photonic qubits, *Rev. Mod. Phys.* **79**, 135 (2007).
- [49] C. Wang, M. Zhang, X. Chen, M. Bertrand, A. ShamsAnsari, S. Chandrasekhar, P. Winzer, and M. Lončar, Integrated lithium niobate electro-optic modulators operating at CMOS-compatible voltages, *Nature* **562**, 101 (2018).
- [50] M. Zhang, C. Wang, Y. Hu, A. Shams-Ansari, T. Ren, S. Fan, and M. Lončar, Electronically programmable photonic molecule, *Nat. Photon.* **13**, 36 (2019).
- [51] C. Reimer, Y. Hu, A. Shams-Ansari, M. Zhang, and M. Loncar, High-dimensional frequency crystals and quantum walks in electro-optic microcombs, arXiv:1909.01303v1.
- [52] A. Dutt, M. Minkov, Q. Lin, L. Yuan, D. A. B. Miller, and S. Fan, Experimental band structure spectroscopy along a synthetic dimension, *Nat. Commun.* **10**, 3122 (2019).
- [53] A. Dutt, Q. Lin, L. Yuan, M. Minkov, M. Xiao, and S. Fan, A single photonic cavity with two independent physical synthetic dimensions, *Science* **367**, 59 (2020).
- [54] D. Hey and E. Li, Advances in synthetic gauge fields for light through dynamic modulation, *R. Soc. Open Sci.* **5**, 172447 (2018).
- [55] L. D. Tzuang, K. Fang, P. Nussenzveig, S. Fan, and M. Lipson, Non-reciprocal phase shift induced by an effective magnetic flux for light, *Nat. Photon.* **8**, 701 (2014).
- [56] I. A. D. Williamson, M. Minkov, A. Dutt, J. Wang, A. Y. Song, and S. Fan, Breaking reciprocity in integrated photonic devices through dynamic modulation, arXiv:2002.04754v1.